




# Enhanced Antibacterial Activity of Highly Biocompatible Polymeric Core–Shell Levofloxacin Gold Nanocomposite Formulation Against *Pseudomonas aeruginosa*

S. Karthick Raja Namasivayam<sup>1</sup> · L. Vigneshwaraprakash<sup>2</sup> · K. Samrat<sup>3</sup> · M. Kavisri<sup>4</sup> · Meivelu Moovendhan<sup>5</sup>  · R. S. Arvind Bharani<sup>6</sup>

Accepted: 8 November 2022 / Published online: 18 November 2022

© The Author(s), under exclusive licence to Springer Science+Business Media, LLC, part of Springer Nature 2022

## Abstract

Using natural and synthetic polymers as the components for the core–shell nanocomposite preparation has received recent attention in biomedicine due to their high biocompatibility, high efficacy, and biodegradability. In this present investigation, chitosan-polyvinyl alcohol core–shell gold nanocomposite was synthesised adopting green science principles followed by fabrication with fluoroquinolone antibiotic levofloxacin (LE-CS-PVA-AuNC). Core–shell nanocomposite was prepared from biogenic gold nanoparticles, chitosan, polyvinyl alcohol polymer mixture, and levofloxacin under optimum conditions, and the synthesised nanocomposite exhibited a highly stable nanoarchitecture. Enhancement of antibacterial activity of the nanocomposite was evaluated against the clinical strain of *Pseudomonas aeruginosa* by determination of growth inhibition, survival rate parameters, and biofilm inhibition rate. Levofloxacin-fabricated core–shell nanocomposite brought about higher growth inhibition than the free levofloxacin, which was confirmed by a notable zone of inhibition, growth inhibition at a lower concentration, rapid biofilm inhibitory rate, and changes in survival growth parameters. In vitro drug release pattern was studied by continuous dialysis, which reveals that the nanocomposite exhibited controlled, sustained release pattern and cumulative release reached almost 98.0% at 72 h. Biocompatibility was studied with human keratinocytes (HaCaT cell line), which was studied by measuring cell viability, oxidative stress marker protein, and genotoxicity. The tested nanocomposite was not inducing any sign of toxicity which was confirmed by no marked impact on cell viability, intracellular reduced glutathione, lipid peroxidase, and lactate dehydrogenase activity. In addition, the nanocomposite has not shown any toxic effect on DNA, and all findings indicate that the synthesised nanocomposite was compatible with human keratinocytes. LE-CS-PVA-AuNC synthesised in the present system adopting green science principles can be used in modern biomedicine as an effective and safe antimicrobial agent due to its high antimicrobial action against wound infection pathogens and its best compatibility with human keratinocytes.

**Keywords** Core–shell nanocomposite · Chitosan · Polyvinyl alcohol · Gold nanoparticles · Levofloxacin · *Pseudomonas aeruginosa*

✉ Meivelu Moovendhan  
moovendhan85@gmail.com

## Introduction

As of late, much consideration has been centred around core–shell nanomaterials in biomedicine fields like imaging, sedate conveyance, and disease treatment, as opposed to impetuses and mechanical applications [1]. There are diverse types or forms of core–shell nanocomposites of multiple sizes and shape metal core–non-metallic shell, metal core–metal shell, polymer core–polymer shell, or polymer core–metal core–shell with unique structural and functional properties. Polymer core–shell nanomaterials dependent on gold, platinum, and palladium are, as a rule, widely examined because their properties especially vary from their bulk materials and display remarkable mechanical, thermal, optical, and electrical properties which could be utilised in the different areas of science and technology [2, 3]. Studies on the expulsion of environmental pollutants [4], antimicrobial properties [5], luminescent properties [6], anticancer activity [7], tissue engineering application [8, 9], and drug delivery [10, 11] with the different polymer core–shell nanomaterials emphatically suggest the potential use in biomedicine, ecological, and modern applications.

In biomedicine, polymer core–shell nanocomposites are alluring medication conveyance frameworks since the medication can be epitomised inside the centre. At the same time, the shell properties can be relegated to upgrade tranquilise conveyance needs. A rich way to deal with such particles is to utilise polymer gels, which have growing properties that rely on conditions, for example pH. Along these lines, growth of the shell and the medication discharge can be focused on happening in the ideal area. Besides, they contemplated the thermodynamic practicality and researched both the physical and concoction boundaries to sedate discharge from the centre shell [12]. Through a blend of auxiliary and liquid reproductions, they can clarify the material science behind polymer core–shell nanoparticles to utilise them in medicate conveyance applications [13].

In recent decades, respectable metal nanoparticles have gotten exceptional consideration due to their potential utility in different fields, for example catalysis, material sciences, overwhelming metal evacuation, pharmaceutical sciences, and biomedical applications [14]. Also, the advancement of gold-based nanomaterials as core–shell nanoparticles, gold nanocomposites, and a half and half bunch has risen as a creative, restorative system for diseases and cancer. Whenever the outside of the nanoparticles is adjusted by practical gatherings or atoms or covered with a slim layer of varied materials (with various constituents), they show improved properties contrasted with the non-functionalised uncoated particles. In this work, gold nanoparticles were synthesised from duckweed — the major aquatic biomass and used to fabricate nanocomposite. Duck weeds were considered a major source of metal nanoparticle synthesis due to the efficacy of accumulation of metals in which high centralisation of tannins makes it a heavenly hotspot for many metal ejection and metal nanoparticle synthesis [15]. Synthesis of various nanostructural bioactive materials from aquatic biomasses has been reported. Munive-Olarte [16] synthesised silver and gold nanoparticles using water hyacinth, which was reported by Rosano-Ortega et al. [17]. A green science approach utilising water hyacinth biomass (WHB) for synthesising copper oxide nanoparticles with a high foe of antimicrobial activity has been reported [18, 19]. Cuervo Blanco and Zea [20] synthesised WHB-impregnated nanoessential  $\text{MnO}_2$  for indigo carmine degradation, and they exhibited the promising adsorption reasonability of WHB lattice stacked  $\text{MnO}_2$  nanoparticles. Silver quantum dots from WHB showed remarkable antibacterial activity against *Escherichia coli* [21]. Cellulose obtained from WHB was used as the hotspot for the amalgamation of silver nanoparticles [22]. In this study, duckweed biomass was chosen for gold nanoparticle synthesis, and the synthesised

nanoparticles were utilised as the hotspot for nanocomposite synthesis. Chitosan-polyvinyl alcohol polymers were selected to synthesise core–shell composite followed by fabricated with gold nanoparticle-levofloxacin nanotranquillise conjugate as core–shell polymer gold–levofloxacin nanocomposite. Levofloxacin is a major fluoroquinolone class of antimicrobial agents against the nosocomial infection-causing pathogens, especially *Pseudomonas aeruginosa*, and the present remedial feeling in treating Pseudomonal disease is principally centred around fluoroquinolones. Its expanded use combined with a sharp ascent in antimicrobial resistance [23]. Hence, the elective methodology uses a transporter framework that can improve mediate conveyance. Nanotechnology standards can be used for the upgrade of action of the existing pharmaceutical operator by improved solvency, focusing on their discharge to the ideal site without influencing non-target cells.

In the current examination, chitosan-polyvinyl alcohol core–shell gold nanocomposite was fabricated using levofloxacin, utilising in situ green science principles. The synthesised composite was assessed for the improved antibacterial action against the pathogenic bacterial strain *Pseudomonas aeruginosa*, followed by biocompatibility appraisal with human keratinocytes. Chitosan and polyvinyl alcohol (PVA) were chosen in this examination to prepare core–shell nanocomposite. Chitosan is a character well-known natural polymer made of glucosamine and N-acetyl glucosamine. It has been utilised in mediate delivery, tissue engineering, and other biomedical applications because of its high adequacy, biocompatibility, and biodegradability [24]. Polyvinyl alcohol (PVA) is a soluble polymer in water and can be used as an excipient for tranquillise conveyance and integrating the platform in tissue engineering [25]. The above-said composite was assessed for an enhanced activity against wound infection bacterial pathogen adopting agar diffusion assay, micro-broth dilution assay, and biofilm inhibition assay.

Further, the nanocomposite impact on endurance rates was concentrated by assurance of decimal decrease time,  $\log L$  and  $\log E$  (extrapolation number), and  $\log N_t/N_0$ . Biocompatibility of the nanocomposite utilising human keratinocytes was checked by estimating cell feasibility, hostile to oxidative chemical status, lactate dehydrogenase (LDH) discharge, and genotoxicity appraisal. An eco-friendly green course methodology received in this current examination may have significant remedial adequacy against deadly twisted disease-causing pathogenic bacterial strains with high viability and biocompatibility.

## Materials and Methods

### Reagents, Chemicals, and Culture Medium

Chemicals and reagents used for the synthesis of core–shell nanocomposite preparation (Chloroauric chloride, Chitosan, Polyvinyl alcohol, and levofloxacin) with high-purity (Analytical grade) were obtained from Sigma-Aldrich. Culture media, including antibiotics used for antibacterial studies and cell culture assays, were purchased from HiMedia, Mumbai, India.

### Synthesis of Gold Nanoparticles

Reduction of the gold precursor into active gold nanoparticles using metabolites present in the biomass extract broth of duck weeds collected from local ponds. Collected biomass was processed into powder form for further studies. Biomass powder thus obtained (0.75 g)

was suspended in 100 mL of deionised water, and the contents were well mixed well. The homogenous suspension thus obtained was boiled in the water bath at 60 °C for 15 min. Boiled biomass suspension was filtered through filter paper (Whatman No. 1) under aseptic conditions, and the collected filtrate (25 mL) was mixed with freshly prepared 2.5 mL of 0.1 M chloroauric chloride solution. The reaction mixture thus prepared was incubated at ambient conditions (29 °C). Conversion of the reaction mixture to dark pink or ruby red colour reveals the gold nanoparticles synthesis—separating the nanoparticles from the reaction mixture by successive centrifugation (15,000×g). Collected pellets were washed thrice with deionised water to remove non-reactive debris. The washed pellet was lyophilised and used for further studies.

### **Levofloxacin-Fabricated CS-PVA Hybrid Polymer Gold Nanocore-Shell Preparation**

The known volume of chitosan (0.25% w/v) that was dissolved in deionised water-acetic acid mixture, and 0.25% of polyvinyl alcohol dissolved in deionised water (PVA), was stirred at room temperature in a magnetic stirrer, followed by the addition of gold nanoparticle suspension (5 mL), and MIC dosage of levofloxacin. Reaction mixture thus prepared was kept under magnetic stirrer at ambient temperature for 3 h. After stirring, the suspension was centrifuged at 10,000×g; the collected pellet was lyophilised and used for further studies.

### **Characterisation**

The reaction mixture thus obtained with synthesised nanoparticles was characterised by major characterisation techniques like UV–visible spectroscopy, Fourier transform infrared spectroscopy (FTIR), atomic force spectroscopy (AFM), and scanning and transmission electron microscopy. Before the characterisation studies, the reaction mixture was purified by successive centrifugation followed by lyophilisation. UV–visible absorption spectrum was taken at 200–800 nm on a Shimadzu spectrophotometer. FTIR analysis was studied with Shimadzu FT-IR8300. Carl-Zeiss field-emission scanning electron microscope and Techni F 12 transmission electron microscope were used to record morphological characters. The topological surface characters were analysed using atomic force microscopy (Ntegra Prima).

### **Antibacterial Activity**

#### **Bacterial Strain Collection and Confirmation**

The antibacterial activity of nanoparticles was contemplated against the human pathogenic bacterial strain *Pseudomonas aeruginosa* isolated from a pyogenic infection patient. The culture was obtained from the Department of Microbiology, SIST Dental College. Standard methods did collection and processing of the samples (pus swabs). Samples which revealed the occurrence of *P. aeruginosa* were confirmed by culture-dependent methods [26]. Swab samples were inoculated in brain heart infusion broth at 37 °C for 24 h. After activation, the inoculum was streaked on MacConkey agar, blood agar, and cetrimide agar. Identification of the strain was made based on distinct morphological characteristics. Followed by cultural characterisation, biochemical tests like catalase, oxidase, IMVIC test, urease test, and triple sugar iron tests were carried out. Molecular characterisation based on 16 s rRNA

analysis was also carried out to confirm the isolated strain. The genomic DNA of the bacterial strain was isolated from the bacterial strain, followed by amplification with 16S rRNA primers. Using NCBI database BLAST analysis, the amplified 16S rRNA sequences were determined. The phylogenetic tree was constructed from this data.

### Antibacterial Susceptibility Testing

The antibacterial activity was initially demonstrated by agar diffusion assay, microbroth dilution assay, and enhanced biofilm susceptibility testing assay. Overnight broth culture of tested bacterial strains was spread on sterile Mueller Hinton agar medium using a sterile swab. Using sterilised gel puncture, agar cups (8 mm) were made; followed by the addition of gold nanoparticles, levofloxacin, and CS-PVA polymer; and nanocomposite fabricated levofloxacin suspension was added (0.1%). Inoculated plates were incubated at 37 °C for 24 h. Triplicates were kept up for every treatment. The zone of inhibition was recorded after the incubation.

Microdilution liquid medium assay was also studied to study antibacterial activity. Overnight broth culture of the tested bacterial strain was exposed to double serial dilution of the sample followed by measuring the growth. The sample's lowest concentration, which inhibited the organism's growth, was considered minimum inhibition concentration (MIC). From the MIC, the minimum bactericidal concentration was determined.

### Determination of Survival Rates

Antibacterial activity of the respective formulation was further studied by determination of survival rates, decimal reduction time, and death curve analysis adopting the modified method of food poisoning technique [27]. Two-hundred-microgram dosage of the respective treatment group was added to the 100-mL sterile trypticase soy broth inoculated with bacterial strain inocula (1 mL). The content present in the flask was gently mixed and kept in the shaker at different time intervals (10, 30, 60, and 120 min) at 37 °C. One millilitre of the cell suspension was transferred from the respective flask into a sterile test tube with phosphate-buffered saline (PBS) and serially diluted. Of the aliquot from the respective treatment, 0.1 mL was spread plated on sterile trypticase soy agar (TSA) plates and incubated at 37 °C for 24 h. Control and three replications were maintained. After the incubation period, the colonies were counted from the respective treatment. The viable count data determined total viability (%) decimal reduction time, lag  $L$  and lag  $E$  (extrapolation number), and  $\log N_t/N_0$ .

### Biofilm Development Inhibition Study Adopting Nitrocellulose Membrane Assay

In this study, nitrocellulose membrane assay did a nanocore-shell-induced biofilmicidal effect. This method allowed bacterial inoculum treated with the respective treatment group to form biofilm on a membrane filter. The biofilm was measured through the spectrophotometric determination of extracted biofilm. The known volume of bacterial inoculum (0.1 mL) was transferred to the sterile Eppendorf tube, followed by the addition of nanocore-shell (0.1% w/v), incubated at 37 °C for 1 h. After the incubation, 0.1 mL of the treated bacterial culture was spot inoculated on a sterile membrane filter that was cut into two equal pieces that were kept in 6-well tissue culture plates. The seeded plate was covered and incubated at 37 °C for 72 h. The control group is composed of bacterial culture

only. Every 12-h intervals, the filter was taken. After the period of incubation, the inoculated filter was taken, and the biofilm inhibition assay was carried out by a new modified method of spectrophotometric inhibition assay as described earlier. Morphology of biofilm in the respective treatment was analysed by scanning electron microscopy. As reported in our previous study, the isolation of adherent biofilm was followed by processing for SEM analysis.

### **In Vitro Drug Release**

A controlled or sustained release pattern of levofloxacin from the nanoformulation was studied under laboratory conditions using the dialysis bag method. In this method, a lyophilised form of polymer core–shell nanocomposite was suspended in different solvents, including deionised water, followed by dialysis using a specific pore-size dialysis membrane against physiological saline. Dialysis was done at 37 °C under a magnetic stirrer. The dialysis medium was collected at a determined time intervals, followed by filtration using a syringe filter under aseptic conditions. The absorbance of the dialysate was measured at 288 nm.

**Biocompatibility Studies.** Biocompatibility of the synthesised nanocomposite was evaluated against HaCaT (human keratinocytes) cell line by determination of nanocomposite-induced cell toxicity, antioxidative enzyme status (intracellular glutathione, lipid peroxidase), lactate dehydrogenase (LDH), and reactive oxygen species (ROS) generation.

### **Cell Viability**

Nanocomposite-induced cytotoxicity on the HaCaT cell line was studied by tetrazolium dye–MTT assay [28]. Cells grown in a suitable cell medium — Dulbecco modified Eagle medium (DMEM)/F-12 medium — were exposed to nanocomposite samples with different concentrations and incubated under optimum conditions. Free gold nanoparticles, free levofloxacin, and CS-PVA copolymers were used to check the efficacy. Respective treatment groups after specific incubation period were added with MTT-(3-(4,5-dimethyl thiazole-2-yl)-2,5-diphenyltetrazolium bromide) solution (0.5 mg/mL incubated at 37 °C for 4 h). After the incubation period, 0.1 mL of dimethyl sulphoxide (DMSO) was added, followed by measuring optical density at 570 nm using an ELISA reader. Control and triplicates were maintained. Cell viability was calculated by finding the differences in optical density of nanocomposite-treated cells and control group cells.

### **Evaluation of Total Cellular Glutathione**

Major antioxidative enzymes reduced glutathione (GSH), and lipid peroxidase was measured in HaCaT cells which were also used to determine the toxic effect of nanocore-shell. Lysate derived from respective treatment group-treated keratinocyte cells was used as the source. Supernatant derived from the lysate thus obtained was mixed with 5,5-dithio-bis-(2-nitrobenzoic acid, glutathione reductase, and NADPH. Spectrophotometric measurement of the reaction end product thus obtained was done at 412 nm. The concentration of total cellular glutathione (tGSH) was determined from standard GSH.

## Lipid Peroxidase Activity

The impact of nanocomposite on the lipid peroxidase (LPO) activity was studied by measurement of total malondialdehyde (MDA) in the respective treatment group. A reaction mixture composed of cell homogenate in buffer was incubated with reactants. The enzymatic end product — malondialdehyde thus formed — was measured spectrophotometrically and expressed in MDA formed/mg protein nanomoles.

## Lactate Dehydrogenase Release

Nanocomposite-induced lactate dehydrogenase activity was also used to determine the biocompatibility/cell suspension that derived from the respective treatment group was used as the source for this enzymatic assay along with pyruvic acid, reduced nicotinamide adenine dinucleotide (NADH) in phosphate buffer. Absorbance of the enzymatic reaction end-product was measured (340 nm).

## Genotoxicity

The genotoxicity of the nanocomposite was studied to determine biocompatibility. In this method, DNA was extracted from the cultured cells adopting the standard protocol, and the extracted pure DNA (20/mL) was stored in Tris buffer. The known volume of the respective treatment group (100 µg) was added to the isolated DNA and incubated at 37 °C for 2 h. After the exposure, electrophoresis was done using Tris–acetate buffer containing 15 µg/mL ethidium bromide in mini-submarine apparatus at 100 A for 30 min. After electrophoresis, the gel was visualised under a UV transilluminator.

## Statistical Analysis

The *t*-test models analysed the statistical significance of all the experimental data.

## Results and Discussion

In recent years, core–shell-structured nanocomposites are gaining increasing attention due to their unique structures and properties. This unique property makes it a particularly important emerging nanomaterial widely used in various fields like bionanotechnology, optics, electroluminescence devices, and bioimaging energy storage materials [29]. In this present investigation, the enhanced antibacterial activity of fluoroquinolone-based levofloxacin antibiotic-fabricated chitosan-polyvinyl alcohol core–shell gold nanocomposite was prepared by in situ green science principle against major wound infection causing bacterial pathogen *Pseudomonas aeruginosa* and its compatibility towards human keratinocytes was studied.

## Synthesis of Gold Nanoparticles

In one eco-friendly course, biocompatible gold nanoparticles were synthesised from WH biomass water extricate stock. Essential affirmation of gold nanoparticle amalgamation in WHB water extract broth was seen by the broth change into ruby red, demonstrating the

synthesis of gold nanoparticles. Recording a sharp plasmon absorption peak at 542 nm uncovers the synthesis of gold nanoparticles in duckweed water extract (Fig. 1). Natural phytochemicals in the plants mediate the green synthesis of metallic nanoparticles by diminishing the metal trailblazers into bioactive nanoparticles. After this preliminary confirmation, the collected nanoparticles were used for further studies.

### Synthesis of Polymer Core–Shell Gold Nanocomposite Fabricated With Levofloxacin

In situ green science principles were adopted to synthesise levofloxacin-fabricated chitosan-polyvinyl alcohol core–shell gold nanocomposite. Selected analytical techniques studied the structural and functional properties of the nanocomposite. Preliminary confirmation was done by UV–visible absorption spectroscopy, and the UV–visible absorption spectra in Fig. 2 show the characteristic interaction of polymer core–shell gold nanocomposite

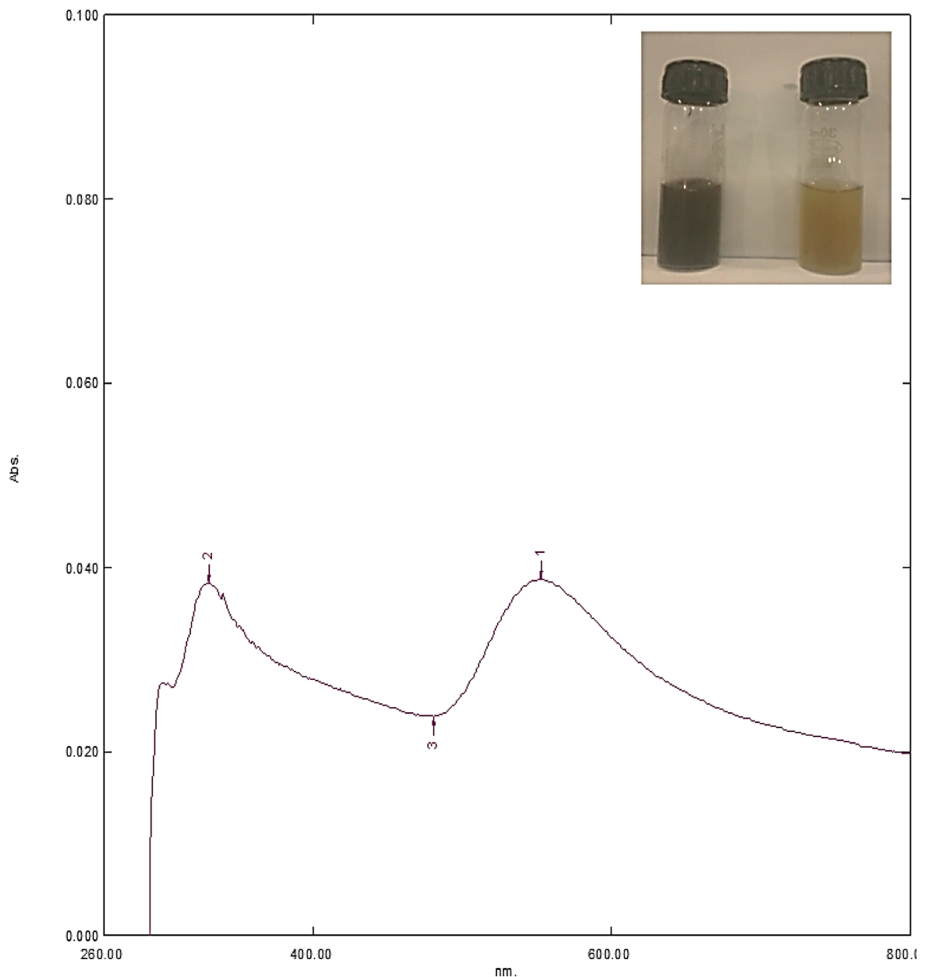


**Fig. 1** UV–visible absorption spectra of synthesised gold nanoparticles



with levofloxacin. Primarily, the wavelength of the surface plasmon band shows a notable shift of surface plasmon resonance. But the absorption band stabilises at 545 nm as confined to gold nanoparticles. Slight asymmetrical absorption bands at 288, 339, and 361 nm indicate the presence of other components involved in fabrication, like polymers and antibiotic levofloxacin. The FTIR analysis was used to determine the functional group. The FTIR spectra in Fig. 3 show the prominent peaks at  $3432.35\text{ cm}^{-1}$  corresponding to the polymeric functional group. Peaks at approximately  $2044.52\text{ cm}^{-1}$  represent N–H stretching vibration. Peaks at  $1633.03\text{ cm}^{-1}$  represent N–H bending, and a peak at  $1384.37\text{ cm}^{-1}$  represents O–H bending and C–H stretching. A peak is also observed at  $1091.66\text{ cm}^{-1}$  showing C–O–C stretching in the polysaccharide of chitosan. A weak absorption band at  $2924.7\text{ cm}^{-1}$ , which corresponds to the levofloxacin function group, clearly indicates that the levofloxacin drug conjugate interacts with polymeric-gold nanocomposite.

Structural properties were further carried out with electron microscopy studies. SEM micrograph revealed agglomerated, rough, electron-thick polymeric core-shell structure ranging from 33 to 46  $\mu\text{m}$  (Fig. 4a). EDAX analysis confirms the elemental composition of composite by showing a strong signal from the respective elements involved in core-shell polymer composite formation (Fig. 4b). TEM micrograph depicted in Fig. 4c shows that electron-dense chitosan-polyvinyl alcohol polymeric core-shell attached to the Au-LF

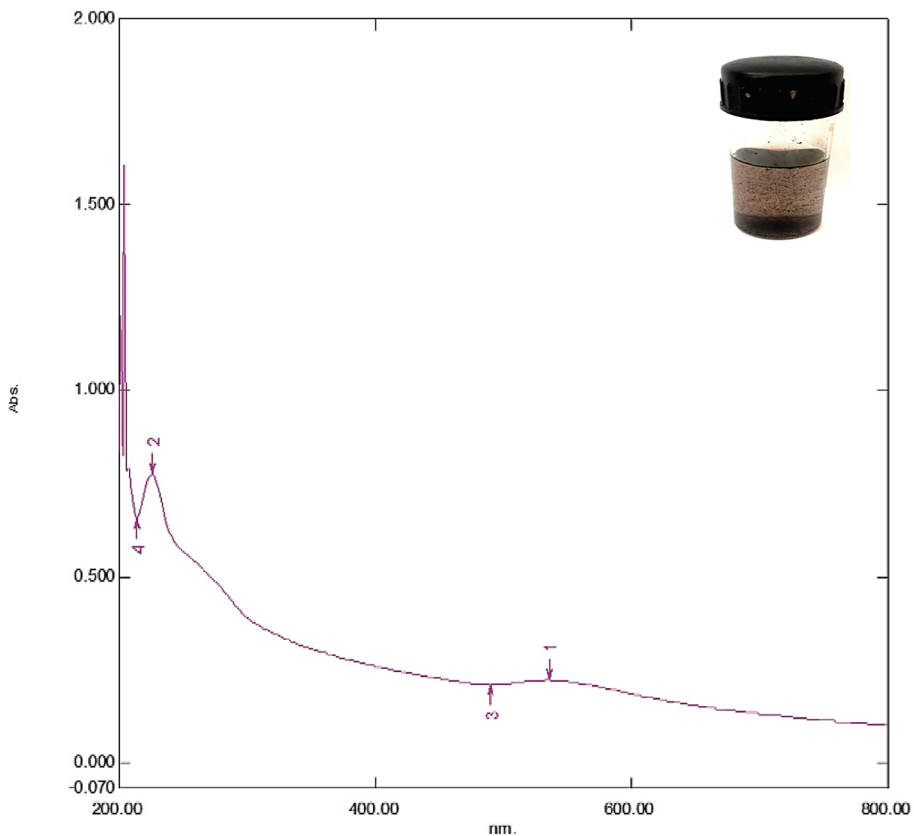


**Fig. 2** UV-visible absorption spectra of LE-CS-PVA-AuNC

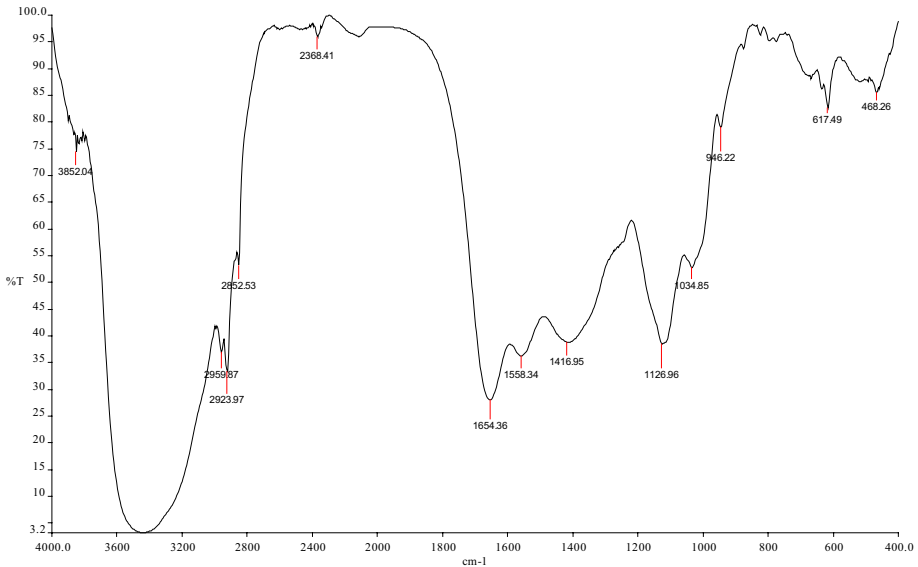


**Fig. 3** FTIR spectra of levofloxacin-fabricated CS-PVA core-shell nanocomposite

nanodrug conjugate and transformed into well-dispersive core-shell electron-dense polymer nanocomposite. AFM was utilised as the central technique to screen the disintegration and agglomeration design. The geographical picture of the nanocomposite, specifically splendid spots, uncovers that particular example of composite (Fig. 5). The surface topology of the nanocomposite was examined by AFM, which was contemplated by  $3 \times 3$  mm.

## Antibacterial Activity

### Selection of Bacterial Strain

A total of 43 isolates belonging to three species were isolated from pyogenic infection patients. Isolated three species, *Pseudomonas aeruginosa*, *Proteus* sp., and *Escherichia coli*, were identified based on cultural and biochemical characteristics by adopting suitable culture-dependent methods. Figure 6 depicts the generic composition of bacterial strains. Amongst the three bacterial species, *P. aeruginosa* was found to be dominant (72.0%), and the occurrence was relatively high in a male patient (35–50 years), followed by *Proteus* sp. (19.0%) and *E. coli* (9.0%). Because of the highest occurrence, *P. aeruginosa* was selected for further studies. The results of different biochemical tests to confirm *P. aeruginosa* are shown in Table 1. Identification of the bacterial strain was further confirmed by 16 s rRNA analysis which reveals 99.0% similarity with *P. aeruginosa* (Fig. 7).

### Antibacterial Susceptibility Testing

Antibacterial activity of synthesised nanocomposite was studied against *P. aeruginosa* by measuring zone of inhibition, minimum inhibition concentration (MIC), minimum bactericidal concentration (MBC), determination of survival rates, and biofilm inhibition rates.

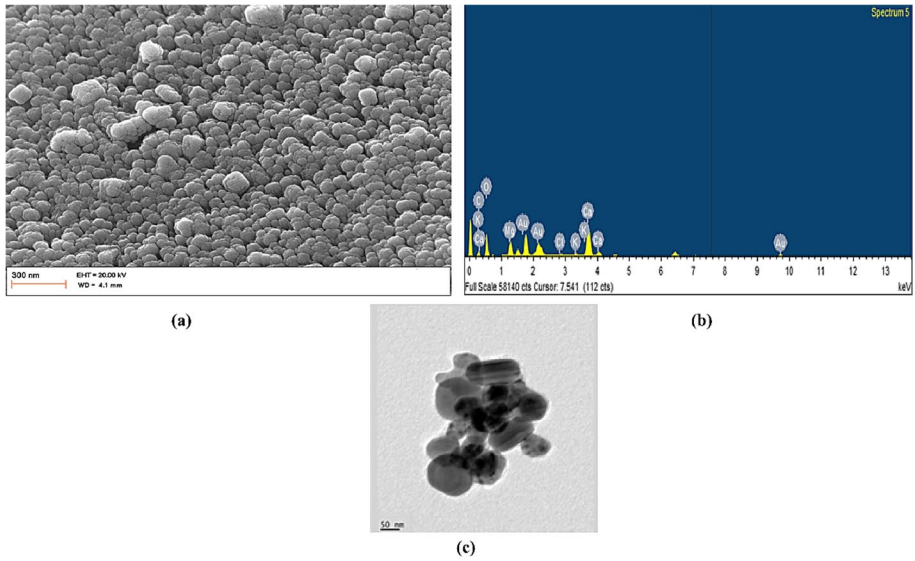


**Fig. 4** Particle morphology studies of levofloxacin-fabricated CS-PVA core-shell nanocomposite: **a** SEM micrograph, **b** EDAX spectra, and **c** TEM micrograph

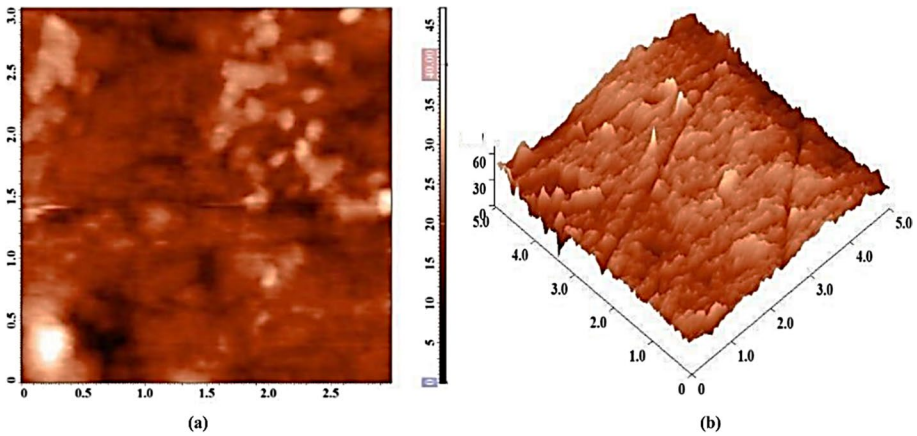


**Fig. 5** Surface topology characterisation of levofloxacin-fabricated CS-PVA core-shell nanocomposite by AFM: **a** 2D micrograph and **b** 3D micrograph

Preliminary determination was studied in well diffusion assay, indicating that free gold nanoparticles and CS-PVA polymer were not recording any notable sign of antibacterial effect (Table 1). As shown in Table 2, it can be seen that levofloxacin-fabricated CS-GA–AuNC shows a higher zone of inhibition than free levofloxacin. Microdilution broth assay was used to decide MIC, and MBC shows that the tested strain was repressed at the lower convergence of levofloxacin-fabricated CS-PVA treatment (Table 3). MIC and MBC of free levofloxacin were found to be 60  $\mu$ g and 80  $\mu$ g, whereas levofloxacin-fabricated CS-PVA

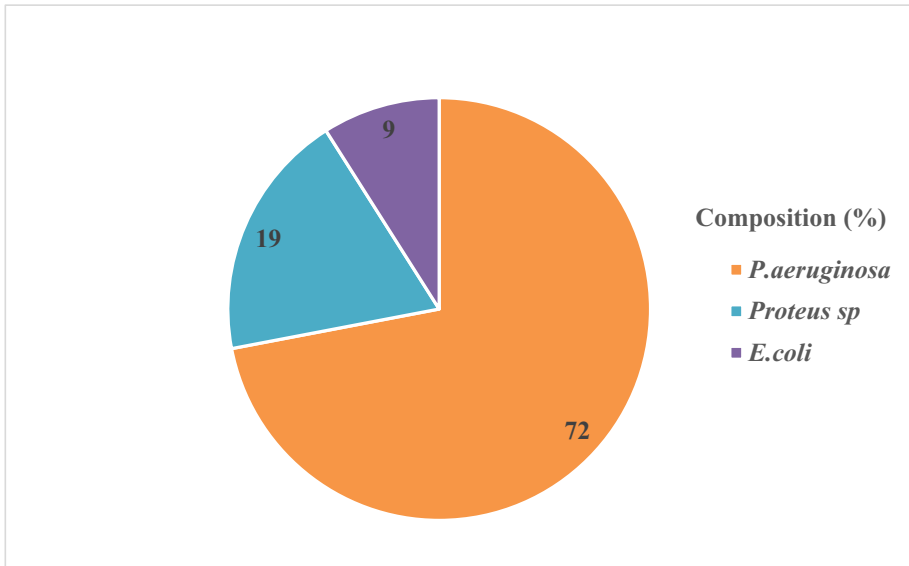


**Fig. 6** Species composition of wound infection pathogenic strains

**Table 1** Morphological and biochemical characteristics of *Pseudomonas aeruginosa*

	Results
Gram reaction	Gram negative, motile, rod
Oxidase test	Positive
Catalase test	Positive
Indole test	Negative
Methyl red	Negative
Voges-Proskauer	Negative
Simmon citrate test	Positive
Urease test	Negative
Oxidative-fermentation (O-F) test	Negative
Glucose (acid with gas)	
Lactose (acid with gas)	Negative
Sucrose (acid with gas)	Negative
Hydrogen sulphide production	Negative

reveals 30 and 40 µg. Our present finding was supported by the previous report, which reveals the notable antibacterial activity of chitosan-polyvinyl alcohol blend nanofibres [30].

Enhancement of antibacterial activity was further studied by determination of survival rate parameters like total viability (%), decimal reduction time, lag *L* and lag *E* (extrapolation number), death curve analysis, and log  $N_t/N_0$  of tested bacterial strains. Data obtained from changes in the total viable count of bacterial strains treated with

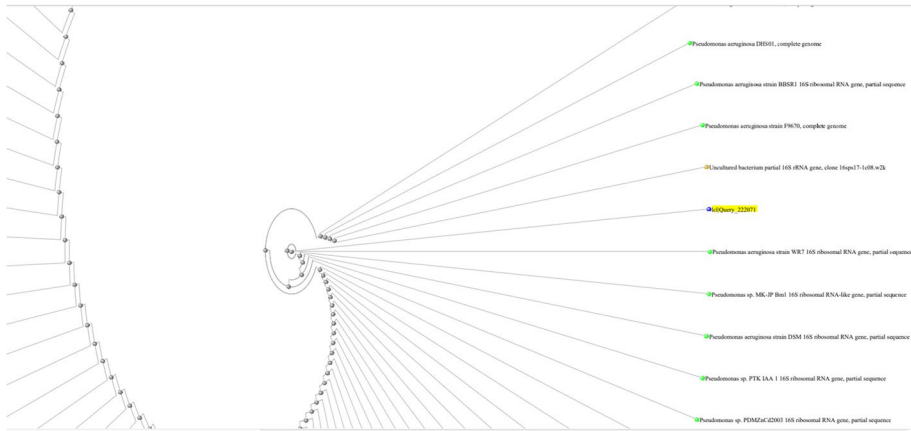


**Fig. 7** Phylogenetic tree of *Pseudomonas aeruginosa*

**Table 2** Zone of inhibition of levofloxacin-fabricated polymer core–shell AuNC against *P. aeruginosa*

Treatment	Zone of inhibition (mm)
Free gold nanoparticles (F-AuNPs)	0.0
Free levofloxacin (F-LF)	18.0
CS-PVA polymer mixture (CS-PVA)	0.0
Levofloxacin-fabricated chitosan-polyvinyl alcohol core–shell AuNC (LF-CS-PVA-AuNC)	31.0*

\*Statistically significant at 0.5% level by DMRT

**Table 3** Minimum inhibition concentration (MIC) and minimum bacteriicidal concentration (MBC) of nanocomposite against *P. aeruginosa*

Treatment	MIC (µg)	MBC (µg)
Free levofloxacin (F-LF)	60.0	80.0
Levofloxacin-fabricated CS-PVA polymer core–shell nanocomposite	30.0*	40.0*

\*Statistically significant at 0.5% level by DMRT

nanocomposite was shown in Fig. 8, which indicates that a significant reduction of total viability was recorded in nanocomposite treatment ( $P=0.5\%$ ). The noteworthy decline of viability was observed in nanocomposite treatment in a time-dependent manner. These results show that levofloxacin-fabricated nanocomposite exhibited an enhanced antibacterial activity against the tested bacterial strain, confirmed by the effective reduction of viability. The effect of nanocomposite on the decimal reduction time (DRT) — time required for a 90% decline in the number of viable cells — was presented in Fig. 9, revealing that levofloxacin treatment exhibited notable DRT, which was significantly different from other treatment groups. Determination of lag ( $L$ ) and log extrapolation numbers ( $E$ ) was also studied from the total count, and the results shown in Fig. 10

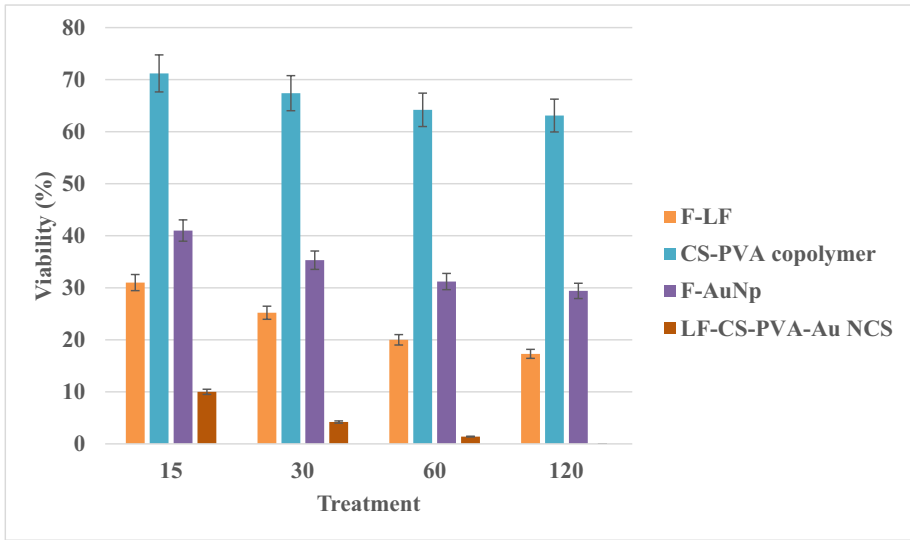


**Fig. 8** Effect on the viability (%) at different time intervals (min)

indicate that nanocomposite exhibited significant variation in lag *L* and log *E*. Levofloxacin-fabricated nanocomposite treatment brought about lower lag *L* and higher log *E* than other treatment groups. From the results, levofloxacin-fabricated nanocomposite exhibited prolonged time for the initial growth (lag phase) and reduced log *E* (active phase), which may be due to the controlled or sustained release of levofloxacin and facilitates interaction with viable cells of the tested pathogenic strains which are used to fight against the bacterial cells.

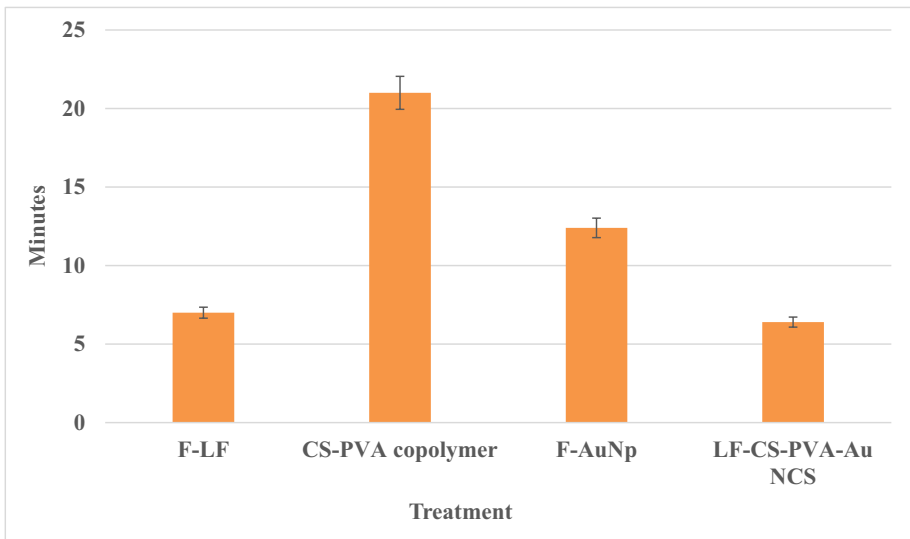


**Fig. 9** Effect on the decimal reduction time (min) of *P. aeruginosa*

Further,  $\log N_t/N_0$  shows negative slope. Cove and Holland [31] reported that microorganisms exposed to toxic agents usually show logarithmic death with or without a shoulder. A  $\log N_t/N_0$  plot against time gives a straight-line graph with a negative slope. The length of the shoulder; the slope of the curve, which is used to calculate the DRT; and the intercepts of the curves are all measurements of resistance of the cells to the agent.

Antibacterial susceptibility of prepared nanocomposite was demonstrated by biofilm inhibition assay—some group of microorganisms' structure biofilm or cell totals in light of unmistakable bacterial correspondence framework. Therefore, biofilm framed by pathogenic strains is considered a significant harmful factor. Biofilm advances bacterial infection by opposing antibiotic treatment because of its relative impermeability [32, 33]. A nitrocellulose membrane-mediated biofilm inhibition assay was done in this present examination. Nanocomposite initiated hostile to biofilm impact was estimated by an assurance of optical density of ethanol-solubilised biofilm treated with respective treatment group utilising spectrophotometry analysis (570 nm). Results demonstrate that nanocomposites were initiated against biofilm impact and the inhibitory rate was seen to expand in increased incubation period. Figure 11 shows that the optical density of extracted biofilm from the bacterial strain uncovers that nanocomposite treatment realised a massive decrease in optical density ( $P=0.05\%$ ). An optical density reduction was seen as the incubation period was prolonged.

Further, the viability of cells isolated from biofilm of tested strain was also studied by adopting a culture-dependent method. Data obtained from the total count reveals the effect of nanocomposite on viability. Results indicate that the nanocomposite treatment brought about a drastic viability reduction (Fig. 12).

Nanoparticles intervened hostile to biofilm or against biofouling impact has been accounted for our present finding on silver, and silica nanoparticles interceded hostile to biofilm or against biofouling viability against biofilm or biofouling system related with genuine water supplies of Chennai, Tamil Nadu, India has emphatically uncovered a compelling job of nanotechnology standards as an enemy of biofouling or against

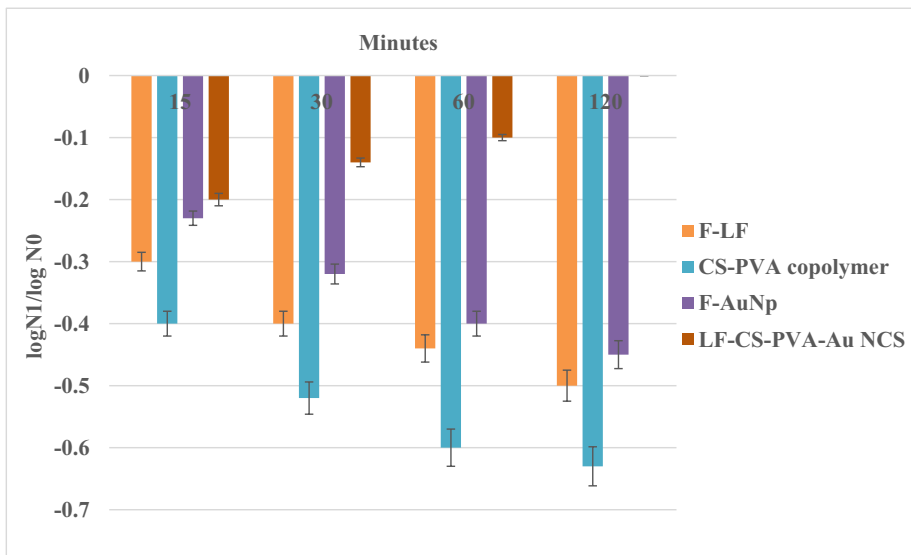


**Fig. 10** Effect of levofloxacin-fabricated CS-PVA core-shell AuNC on  $\log N_t/\log N_0$

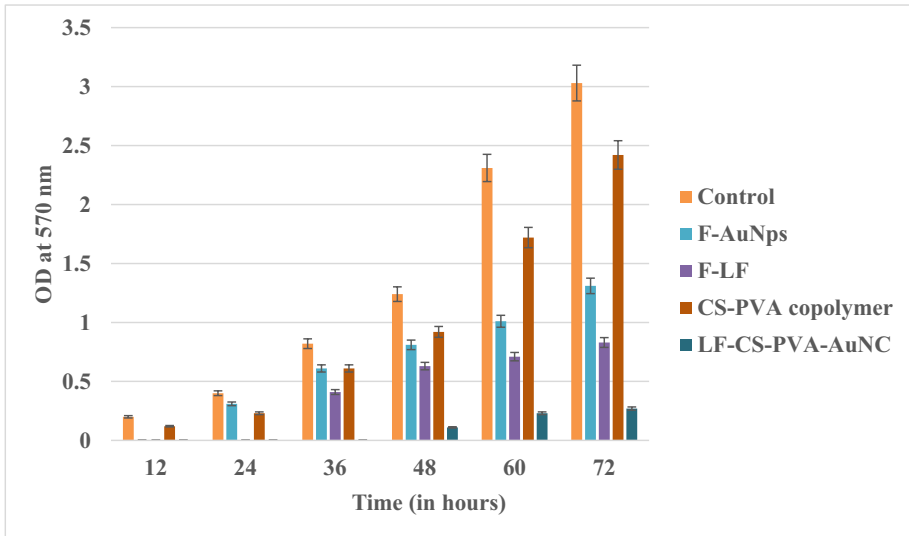


**Fig. 11** Optical density of ethanol-solubilised biofilm of *P. aeruginosa* at different time intervals

biofilm methodology [34]. Viability of further affirmation of hostile to biofilm adequacy of nanocomposite was contemplated by scanning electron microscopy (SEM) investigation. SEM micrograph shows that biofilm development of tested bacterial strain was exceptionally upset (Fig. 13). Nanocomposite initiated hostile to biofilm impact was effectively distinguished by misfortunes in auxiliary respectability of the biofilm. Changes in the basic uprightness caused debilitating or crumbling of cell aggregates.

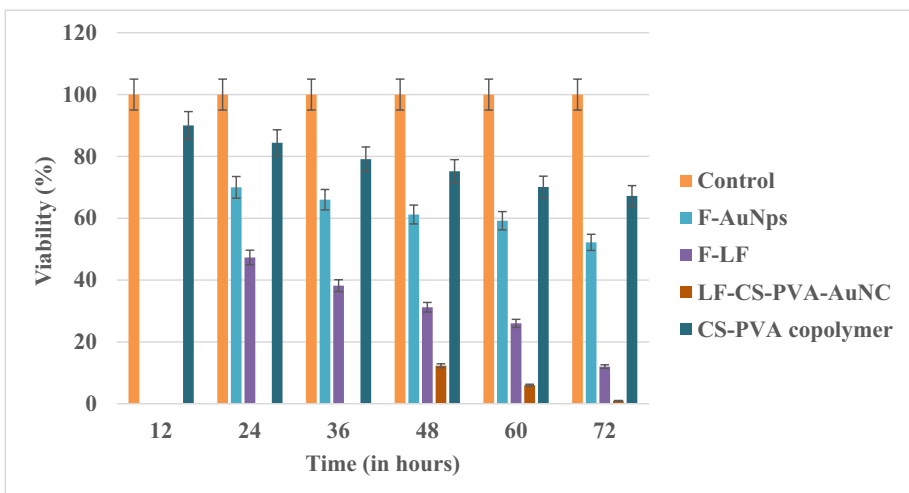


**Fig. 12** Viability of cells of *P. aeruginosa* at different time intervals



## In Vitro Drug Release

The dialysis bag procedure was adopted to study the release profile, which was done by spectrophotometric measurement of drug release at predetermined periods (every 6-h interval till 72 h). The release profile was represented as a percentage, as shown in Fig. 14, which reveals that the release rate in all the solvents was increased gradually at increased time periods which provide the possibility to fight continually against infection resulting in reduced bacterial cell viability.

## Biocompatibility Studies Using Human Skin Keratinocyte (HaCaT Cell Line)

Biocompatibility of synthesised nanocomposite was studied with human skin cells (HaCaT cell line) by determination of cell viability, antioxidative enzymes, lactate dehydrogenase release, reactive oxygen species generation, and genotoxicity which reveals the possible mechanism through which the synthesised nanocomposite exhibits their toxic effect on these cells. Cell viability was studied by MTT assay, which reveals that all the tested dosages of nanocomposite did not induce any cytotoxicity (Fig. 15). The notable impact on the viability was not affected by the treatment's maximum dosage (200 µg). Microscopic examination of the cells treated with different dosages shows that nanocomposite did not induce any undesirable changes in the cell morphology or architecture (Fig. 16). Cell shrinkage, cell count reduction, and nuclear fragmentation were not observed in the nanocomposite treatment group, revealing that the tested nanocomposite was compatible with the keratinocytes. Biocompatibility was further studied by measuring intracellular reduced glutathione (rGSH) and lipid peroxidase (LPO). Determination of rGSH and LPO levels are the biomarkers of oxidative stress which progressively leads to cell death [35]. No significant changes were observed when the cells were exposed to the respective treatment group (Figs. 17 and 18). No marked induction in rGSH and LPO of treated cells reveals that the nanocomposite has not shown any undesirable effects. Measuring lactate dehydrogenase (LDH) is also crucial in confirming cytotoxicity. An increase in LDH indicates injury to the cell membrane. When the tested cells were exposed to the respective treatment group, no marked changes in LDH were recorded, which clearly indicates that the tested nanocomposite was compatible with the cells (Fig. 19). A genotoxicity study was also done to demonstrate biocompatibility. DNA damage leads to carcinogenesis

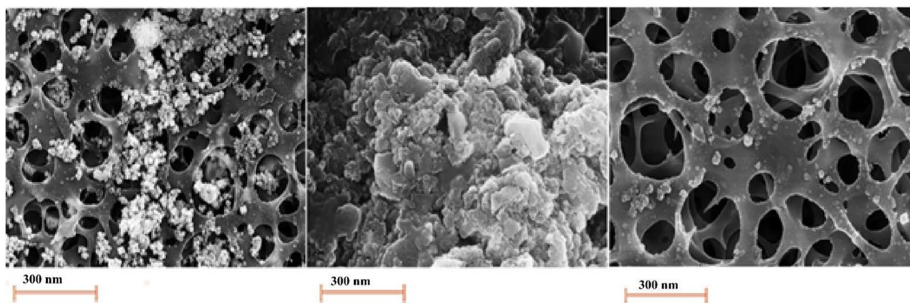


**Fig. 13** SEM micrograph of biofilm of *P. aeruginosa*: **a** free levofloxacin, **b** control, and **c** levofloxacin-fabricated CS-PVA core-shell AuNC

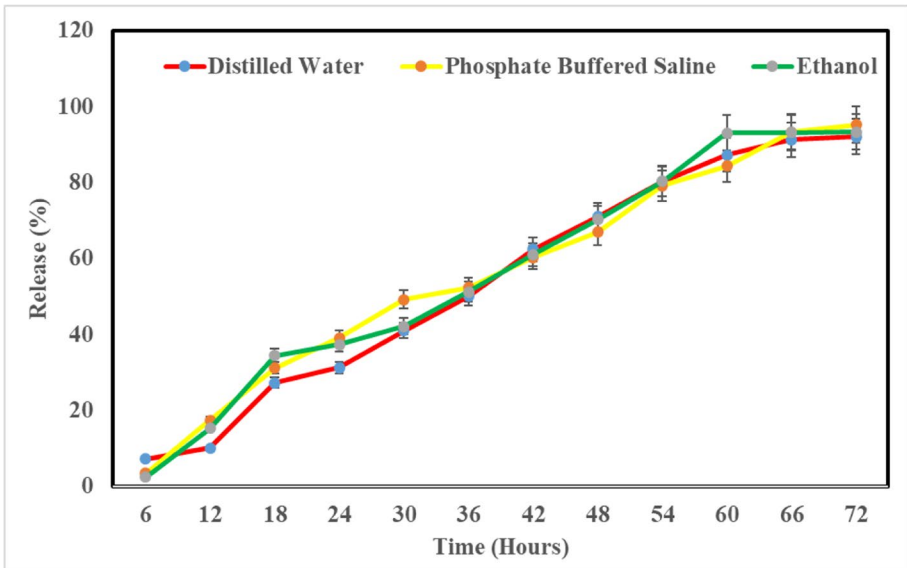


**Fig. 14** Controlled release pattern of levofloxacin from core-shell AuNC

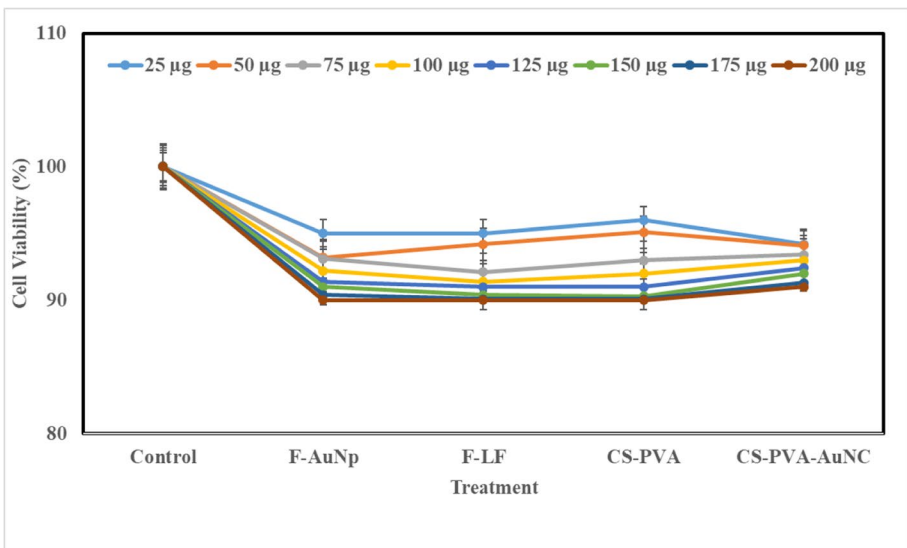


**Fig. 15** Cell viability of human keratinocytes (HaCaT cell line) treated with levofloxacin-fabricated CS-PVA-AuNC

or cell death. The reactive oxygen species (ROS) are known to cause purine, pyrimidine damage, and DNA backbone, leading to genomic toxicity. In this study, genotoxicity was determined by recording DNA fragmentation or degradation. The tested nanocomposite was not inducing genotoxicity which was inferred from the agarose gel electrophorogram depicted in Fig. 20. Nanocomposite treatment did not cause DNA

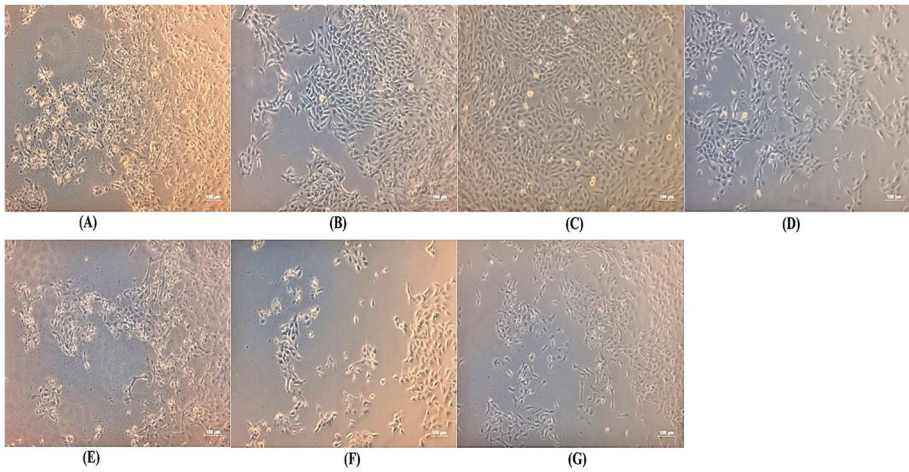


**Fig. 16** Microscopic examination of human keratinocytes (HaCaT cell line) treated with levofloxacin-fabricated CS-PVA-AuNC

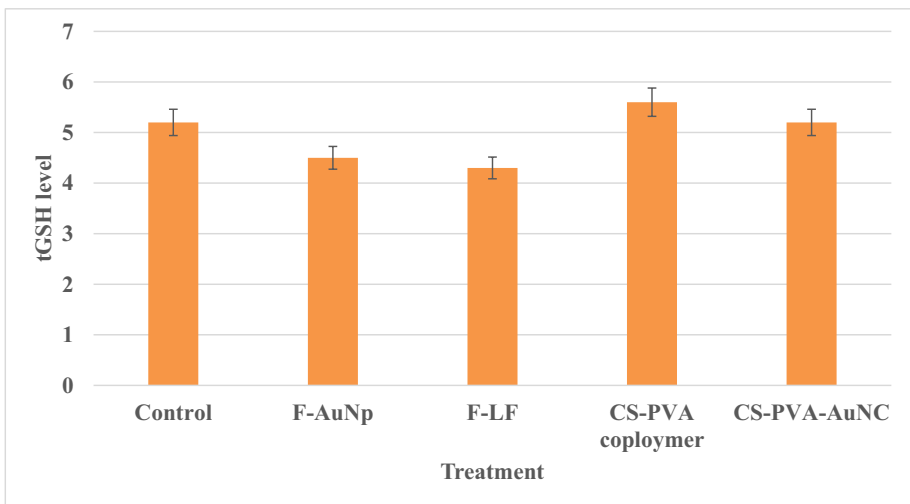


**Fig. 17** Effect of levofloxacin-fabricated CS-PVA-AuNC on reduced glutathione

fragmentation or DNA degradation as in other treatment groups. A clear, sharp, or thick DNA band was observed as in the control group. All these present findings indicate that the synthesised nanocomposite was not inducing any notable effect on cell viability, oxidative stress, and genotoxicity. Figure 21 shows the flow diagram of the proposed work that demonstrates the antibacterial activity and enhanced biocompatibility of antibacterial antibiotic levofloxacin formulated with chitosan-PVA core-shell gold nanocomposite. These results show that the synthesised nanocomposite exhibited

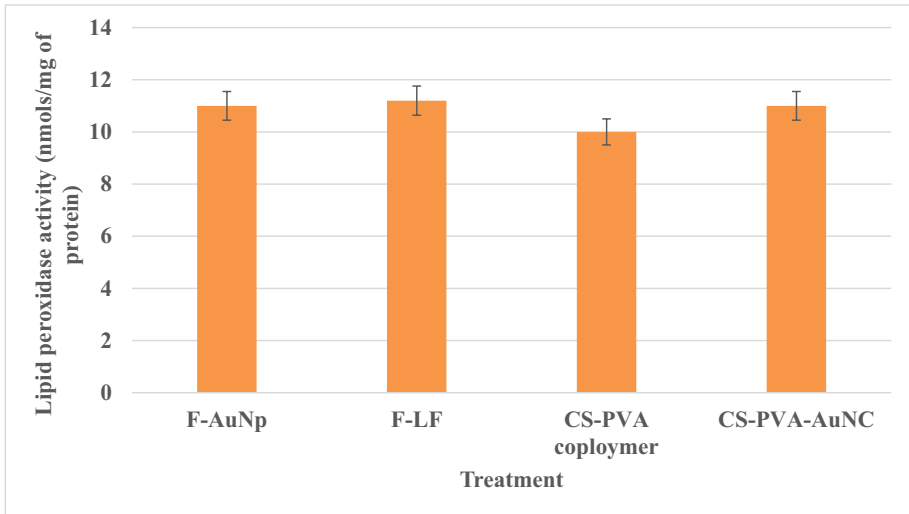


**Fig. 18** Effect of levofloxacin-fabricated CS-PVA-AuNC on lipid peroxidase activity

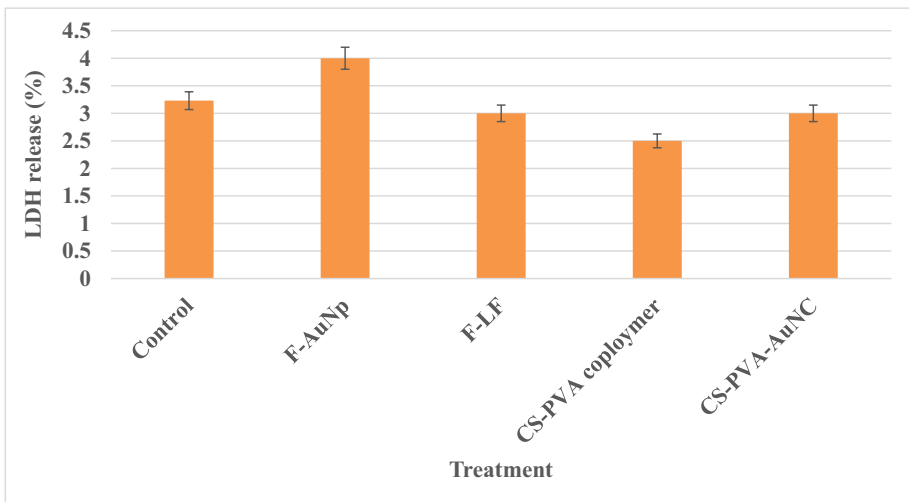


**Fig. 19** Effect of levofloxacin-fabricated CS-PVA-AuNC on LDH release

the best biocompatibility with the human keratinocytes. Further studies using suitable model would suggest the possible utilisation as an effective, safe antimicrobial agent against wound infection-causing organisms.

**Fig. 20** Effect of levofloxacin-fabricated CS-PVA-AuNC on DNA fragmentation (lane 1 — DNA ladder, lane 2 — control, lane 3 — free gold nanoparticles, lane 4 — free levofloxacin, lane 5 — CS-PVA copolymer, lanes 6 and 7 — LF-fabricated CS-PVA-AuNC)

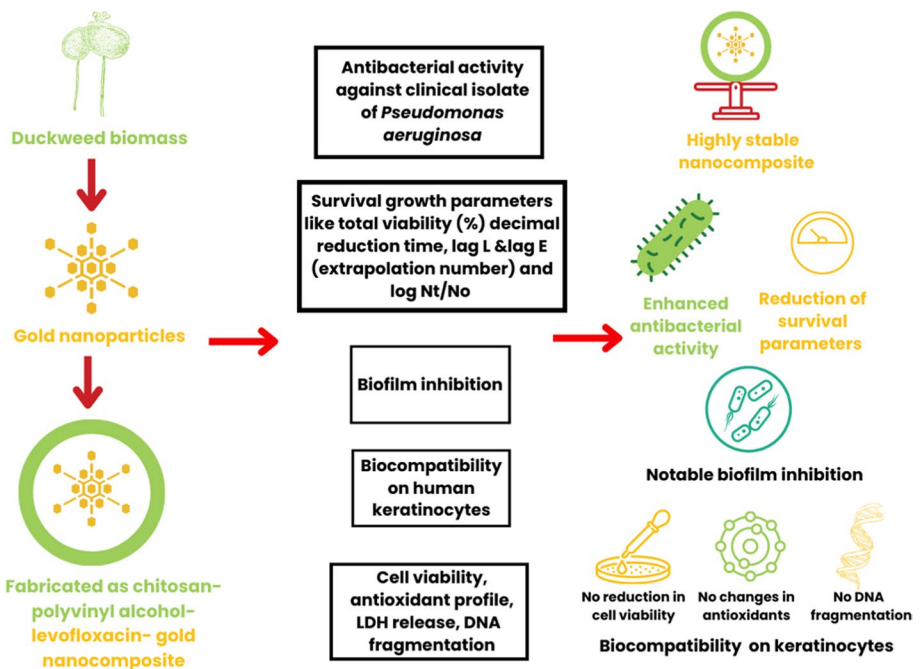
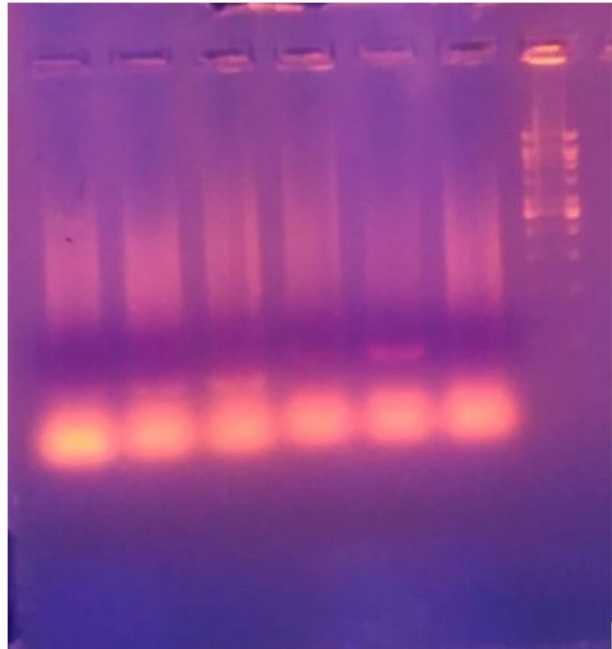


**Fig. 21** Flow diagram of the proposed work

## Conclusion

Polymer core–shell nanocomposite principles are extensively utilised in biomedicine due to their high efficacy and biocompatibility. In this study, chitosan-polyvinyl alcohol polymer core–shell Au nanocomposite fabricated levofloxacin was synthesised by in situ green science principles, which brought about highly stable structural and functional stability with notable nanoarchitecture. Synthesised nanocomposite brought about notable antibacterial activity against antibiotic-resistant strain *P. aeruginosa*—a pathogenic strain isolated from wound infection patients by recording a marked impact on growth or survival parameters and biofilm inhibition. Drug release studies also indicate that the nanocomposite exhibited sustained or controlled release. The synthesised nanocomposite was shown to have the best biocompatible effect on human keratinocytes (HaCaT cells) by recording no marked impacts on cell viability, oxidative enzymes, and DNA. These results show that the nanocomposite prepared in the present system can be used in biomedicine as an effective antibacterial agent against wound infection pathogens.

**Acknowledgements** Centre for Nanoscience & Nanotechnology, SIST, Chennai, was acknowledged for the characterisation studies.

**Author Contribution** S. K. R. N., M. M.: conceptualisation, data curation, supervision, writing — review and editing; L. V.: supervision, writing — review and editing; K. S.: data curation, conceptualisation; M. K.: project administration, validation, writing — original draft; R. S. A. B.: supervision, validation, conceptualisation.

**Data Availability** Data is available on request from the authors.

## Declarations

**Ethical Approval** In this study, the animal experiment was not applicable.

**Consent to Participate** In this study, animals and human trials are not applicable.

**Consent for Publication** Not applicable.

**Competing Interests** The authors declare no competing interests.

## References

1. Shah, N., & Gul, S. (2019). Mazhar Ul-Islam, Core-shell molecularly imprinted polymer nanocomposites for biomedical and environmental applications. *Current Pharmaceutical Design*, 25, 3633–3644. <https://doi.org/10.2174/1381612825666191009153259>
2. Wei, S., Wang, Q., Zhu, J., Sun, L., Lin, H., & Guo, Z. (2011). Multifunctional composite core-shell nanoparticles. *Nanoscale*, 3, 4474–4502. <https://doi.org/10.1039/c1nr11000d>
3. Saleh, H. H., Ali, Z. I., & Afify, T. A. (2016). Synthesis of Ag/PANI core-shell nanocomposites using ionizing radiation. *Advances in Polymer Technology*, 35, 335–344. <https://doi.org/10.1002/adv.21560>
4. Ramesh, A., Tamizhdurai, P., Gopinath, S., Sureshkumar, K., Murugan, E., Shanthi K. (2019). Facile synthesis of core-shell nanocomposites Au catalysts towards abatement of environmental pollutant Rhodamine B, Heliyon. 5. <https://doi.org/10.1016/j.heliyon.2018.e01005>.
5. Dobrucka, R., & Dlugaszewska, J. (2018). Antimicrobial activity of the biogenically synthesised core-shell Cu@Pt nanoparticles. *Saudi Pharmaceutical Journal*, 26, 643–650. <https://doi.org/10.1016/j.jsps.2018.02.028>

6. Y. Qiao, W. Li, J. Bao, Y. Zheng, L. Feng, Y. Ma, K. Yang, A. Wu, H. Bai, Y. Yang, Controlled synthesis, and luminescence properties of core-shell-shell structured  $\text{SiO}_2$ @AIPA-S-Si-Eu@ $\text{SiO}_2$  and  $\text{SiO}_2$ @AIPA-S-Si-Eu-phen@ $\text{SiO}_2$  nanocomposites. *Scientific Reports* 10 (2020). <https://doi.org/10.1038/s41598-020-60538-w>.
7. Cortese, B., D'Amone, S., Testini, M., Ratano, P., Palamà I.E. (2019). Hybrid clustered nanoparticles for chemo-antibacterial combinatorial cancer therapy, *Cancers (Basel)*. 11. <https://doi.org/10.3390/cancers11091338>.
8. W. Su, Y. Hu, M. Zeng, M. Li, S. Lin, Y. Zhou, J. Xie, Design and evaluation of nano-hydroxyapatite/poly(vinyl alcohol) hydrogels coated with poly(lactic-co-glycolic acid)/nano-hydroxyapatite/poly(vinyl alcohol) scaffolds for cartilage repair, *Journal of Orthopaedic Surgery and Research* 14 (2019). <https://doi.org/10.1186/s13018-019-1450-0>.
9. Fathollahipour, S., Abouei Mehrizi, A., Ghaee, A., Koosha, M. (2015). Electrospinning of PVA/chitosan nanocomposite nanofibers containing gelatin nanoparticles as a dual drug delivery system. *Journal of Biomedical Materials Research - Part A*. 103, 3852–3862. <https://doi.org/10.1002/jbm.a.35529>.
10. Rabel, A. M., Namasivayam, S. K. R., Prasanna, M., & Bharani, R. S. A. (2019). A green chemistry to produce iron oxide–chitosan nanocomposite (CS-IONC) for the upgraded bio-restorative and pharmacotherapeutic activities — Supra molecular nanoformulation against drug-resistant pathogens and malignant growth. *International Journal of Biological Macromolecules*, 138, 1109–1129. <https://doi.org/10.1016/j.ijbiomac.2019.07.158>
11. Dabbagh, A., Hedayatnasab, Z., Karimian, H., Sarraf, M., Yeong, C. H., Madaah Hosseini, H. R., & Rahman, N. A. (2019). Polyethylene glycol-coated porous magnetic nanoparticles for targeted delivery of chemotherapeutics under magnetic hyperthermia condition. *International Journal of Hyperthermia*, 36(1), 104–114. <https://doi.org/10.1080/02656736.2018.1536809>
12. Kumar, K. S., Kumar, V. B., & Paik, P. (2013). Recent advancement in functional core-shell nanoparticles of polymers: Synthesis, physical properties, and applications in medical biotechnology. *J. Nanoparticles*, 2013, 1–24. <https://doi.org/10.1155/2013/672059>
13. Vijayalekshmi, V. (2015). UV-visible, mechanical and antimicrobial studies of chitosan-montmorillonite clay/ $\text{TiO}_2$  nanocomposites, *Research Journal of Recent Sciences* 1–5.
14. Borah, D., Hazarika, M., Tailor, P., Silva, A. R., Chetia, B., Singaravelu, G., & Das, P. (2018). Starch-templated bio-synthesis of gold nanoflowers for in vitro antimicrobial and anticancer activities. *Applied Nanoscience*, 8, 241–253. <https://doi.org/10.1007/s13204-018-0793-x>
15. Mahmood, T., Hussain, S. T., & Malik, S. A. (2010). New nanomaterial, and process for the production of biofuel from metal hyper accumulator water hyacinth, African. *Journal of Biotechnology*, 9, 2381–2391. <https://doi.org/10.5897/AJB2010.000-3047>
16. Munive-Olarte, A., Rosano-Ortega, G., Schabes-Retchkiman, P., Martinez-Gallegos, M.S.M., El Kassis, E., Gonzalez-Perez, M., Pacheco-Garcia, F. (2017). Assessment of biomass of leaves of water hyacinth (*Eichhornia crassipes*) as reducing agents for the synthesis of nanoparticles of gold and silver. *International Journal of Advanced Engineering Management Science* 3, 364–370. <https://doi.org/10.24001/ijaems.3.4.14>.
17. Rosano-Ortega, G., Avila-Pérez, P., Zavala, G., Santiago, P., Canizal, G., & Ascencio, J. A. (2008). Inorganic nanoparticles induced naturally in water hyacinth: Structural and chemical study. *Journal of Bionanoscience*, 1, 51–59. <https://doi.org/10.1166/jbns.2007.001>
18. Vanathi, P., Rajiv, P., & Sivaraj, R. (2016). Synthesis, and characterisation of *Eichhornia*-mediated copper oxide nanoparticles and assessing their antifungal activity against plant pathogens. *Bulletin of Materials Science*, 39, 1165–1170. <https://doi.org/10.1007/s12034-016-1276-x>
19. Hemalatha, S., & Makeswari, M. (2017). Green synthesis, characterisation, and antibacterial studies of CuO nanoparticles from *Eichhornia crassipes*. *Rasayan Journal of Chemistry*, 10, 838–843. <https://doi.org/10.7324/RJC.2017.1031800>
20. Cuervo Blanco, T., Sierra Ávila, C.A., Zea Ramírez, H.R. (2016). Nanostructured  $\text{MnO}_2$  catalyst in *E. crassipes* (water hyacinth) for indigo carmine degradation, *Rev. Colomb. Química*. 45, 30. <https://doi.org/10.15446/rev.colomb.quim.v45n2.60395>.
21. Silva, A., Martínez-Gallegos, S., Rosano-Ortega, G., Schabes-Retchkiman, P., Vega-Lebrún, C., Albitar, V. (2017). Nanotoxicity for *E. coli* and characterisation of silver quantum dots produced by biosynthesis with *Eichhornia crassipes*, *Journal Nanostructures*. 7, 1–12. <https://doi.org/10.22052/jns.2017.01.001>.
22. Mochochoko, T., Oluwafemi, O. S., Jumbam, D. N., & Songca, S. P. (2013). Green synthesis of silver nanoparticles using cellulose extracted from an aquatic weed; Water hyacinth. *Carbohydrate Polymers*, 98, 290–294. <https://doi.org/10.1016/j.carbpol.2013.05.038>

23. Jankie, S., Adebayo, A., & Pillai, G. (2012). In vitro activity of fluoroquinolones entrapped in non-ionic surfactant vesicles against ciprofloxacin resistant bacteria strains. *Journal of pharmaceutical technology and Drug Research*, 1, 1–5.
24. Hu, L., Zhu, B., Zhang, L., Yuan, H., Zhao, Q., & Yan, Z. (2019). Chitosan-gold nanocomposite and its functionalised paper strips for reversible visual sensing and removal of trace Hg<sup>2+</sup> in practice. *The Analyst*, 144, 474–480. <https://doi.org/10.1039/c8an01707g>
25. Kuo, T. Y., Jhang, C. F., Lin, C. M., Hsien, T. Y., & Hsieh, H. J. (2017). Fabrication and application of coaxial polyvinyl alcohol/chitosan nanofiber membranes. *Open Phys.*, 15, 1004–1014. <https://doi.org/10.1515/phys-2017-0125>
26. Samanta, S., Das, G., Araphder, S. T. (2012). Multi drug resistant *Pseudomonas aeruginosa* from wild hanuman langur in India. *Journal of Biomedical Science* 1, 1–3
27. El Mahmood, A. M., & Doughari, J. H. (2008). Effect of Dettol® on the viability of some microorganisms associated with nosocomial infections. *African J. Biotechnol.* <https://doi.org/10.5897/AJB08.052>
28. Mosmann, T. (1983). Rapid colorimetric assay for cellular growth and survival: Application to proliferation and cytotoxicity assays. *Journal of Immunological Methods*. 55–63. [https://doi.org/10.1016/0022-1759\(83\)90303-4](https://doi.org/10.1016/0022-1759(83)90303-4).
29. Li, L., Zhang, M., Song, S., Yang, B., Wu, Y., & Yang, Q. (2018). Preparation of core/shell structured silicate composite filler and its reinforcing property. *Powder Technology*, 332, 27–32. <https://doi.org/10.1016/j.powtec.2018.03.037>
30. Gholipour, A.K., Bahrami, S.H., Nouri, M. (2009). Chitosan-poly (vinyl alcohol) blend nanofibers: Morphology, biological and antimicrobial properties, E-Polymers. <https://doi.org/10.1515/epoly.2009.9.1.1580>.
31. Cove, J. H., & Holland, K. T. (1983). The effect of benzoyl peroxide on cutaneous microorganisms in vitro. *Journal of Applied Bacteriology*, 54, 379–382. <https://doi.org/10.1111/j.1365-2672.1983.tb02631.x>
32. Parai, D., Islam, E., Mitra, J., & Mukherjee, S. K. (2017). Effect of Bacoside A on growth and biofilm formation by *Staphylococcus aureus* and *Pseudomonas aeruginosa*. *Canadian Journal of Microbiology*, 63, 169–178. <https://doi.org/10.1139/cjm-2016-0365>
33. Karthick, S., Raja. Namasivayam, Roy, E.A. (2013). Enhanced antibiofilm activity of chitosan stabilized chemogenic silver nanoparticles against *Escherichia coli*, *International Journal of Scientific and Research Publication* 1–9.
34. Karthick Raja Namasivayam, S., Francis, A.L., Arvind Bharani, R.S., Nachiyar, C.V. (2019). Bacterial biofilm, or biofouling networks with numerous resilience factors from real water supplies of Chennai and their enhanced susceptibility to biocompatible nanoparticles. *Journal of Cleaner Production* <https://doi.org/10.1016/j.jclepro.2019.05.199>.
35. Alarif, S., Ali, D., Verma, A., Alakhtani, S., Ali, BA. (2013). cytotoxicity, and genotoxicity of copper oxide nanoparticles in human skin keratinocytes cells. *International Journal of Toxicology* 296–307. <https://doi.org/10.1177/1091581813487563>

**Publisher's Note** Springer Nature remains neutral with regard to jurisdictional claims in published maps and institutional affiliations.

Springer Nature or its licensor (e.g. a society or other partner) holds exclusive rights to this article under a publishing agreement with the author(s) or other rightsholder(s); author self-archiving of the accepted manuscript version of this article is solely governed by the terms of such publishing agreement and applicable law.



## Authors and Affiliations

**S. Karthick Raja Namasivayam<sup>1</sup> · L. Vigneshwaraprakash<sup>2</sup> · K. Samrat<sup>3</sup> · M. Kavisri<sup>4</sup> · Meivelu Moovendhan<sup>5</sup>  · R. S. Arvind Bharani<sup>6</sup>**

<sup>1</sup> Department of Research & Innovation, Saveetha School of Engineering, SIMATS Deemed University, Chennai 602195, Tamil Nadu, India

<sup>2</sup> Department of Biotechnology, Sathyabama Institute of Science and Technology, Chennai 600119, Tamil Nadu, India

<sup>3</sup> Department of Biotechnology, M. S. Ramaiah Institute of Technology, Bangalore 560054, Karnataka, India

<sup>4</sup> Department of Civil Engineering, School of Building and Environment, Sathyabama Institute of Science & Technology, Chennai 600119, Tamil Nadu, India

<sup>5</sup> Centre for Ocean Research, Col. Dr. Jeppiaar Research Park, Sathyabama Institute of Science & Technology, Chennai 600119, Tamil Nadu, India

<sup>6</sup> Phi-Psi Laboratories, Chennai 600083, Tamil Nadu, India